

Brief Report

TiO₂/MWCNT/Nafion-Modified Glassy Carbon Electrode as a Sensitive Voltammetric Sensor for the Determination of Hydrogen Peroxide

Rafael Henrique de Oliveira ¹, Daniel A. Gonçalves ² and Diogo Duarte dos Reis ^{1,*}

¹ Institute of Physics, Federal University of Mato Grosso do Sul—UFMS, Campo Grande 79070-900, MS, Brazil; rafael.henrique206@gmail.com

² Faculty of Exact Sciences and Technology, Federal University of Grande Dourados, Dourados 79804-970, MS, Brazil; daniel.araujogoncalves@gmail.com

* Correspondence: diogo.reis@ufms.br

Abstract: In this work we describe a straightforward approach for creating a nanocomposite comprising multiwalled carbon nanotubes (MWCNTs) and titanium dioxide (TiO₂) using the hydrothermal technique, which is then characterized by scanning electron microscope (SEM), energy-dispersive X-ray spectrometer (EDS), X-ray diffraction analysis (XRD), Fourier transform infrared spectroscopy (FTIR), and thermal gravimetric analysis (TGA) to assess its properties. Nafion is employed as a reticular agent for the nanocomposite on the glassy carbon electrode (GCE), creating the MWCNT/TiO₂/Nafion/GCE system. The electrochemical behavior of the system was evaluated using cyclic voltammetry, revealing its remarkable electrocatalytic activity for detecting hydrogen peroxide in water. The developed sensor showcased a broad linear response range of 14.00 to 120.00 μM, with a low detection limit of 4.00 μM. This electrochemical sensor provides a simple and highly sensitive method for detecting hydrogen peroxide in aqueous solutions and shows promising potential for various real-world applications, particularly in H₂O₂ monitoring.

Keywords: hydrogen peroxide; electrochemical sensor; nanocomposite; cyclic voltammetry; TiO₂; MWCNTs



Citation: de Oliveira, R.H.; Gonçalves, D.A.; dos Reis, D.D. TiO₂/MWCNT/Nafion-Modified Glassy Carbon Electrode as a Sensitive Voltammetric Sensor for the Determination of Hydrogen Peroxide. *Sensors* **2023**, *23*, 7732. <https://doi.org/10.3390/s23187732>

Academic Editor: Cristina Ariño

Received: 27 March 2023

Revised: 4 May 2023

Accepted: 8 May 2023

Published: 7 September 2023



Copyright: © 2023 by the authors. Licensee MDPI, Basel, Switzerland. This article is an open access article distributed under the terms and conditions of the Creative Commons Attribution (CC BY) license (<https://creativecommons.org/licenses/by/4.0/>).

1. Introduction

Hydrogen peroxide (H₂O₂) is a simple but significant compound in various applications, such as pharmaceuticals, clinical, environmental, mining, textiles, and food manufacturing. H₂O₂ is a signaling molecule regulating essential biological processes, such as immune cell activation, vascular remodeling, and apoptosis. H₂O₂ is a secondary product of various enzymatic reactions [1–4]. Due to its importance as a regulating molecule, hydrogen peroxide is an excellent model molecule for applications in developing new electrochemical sensors.

Electrochemical methods are the most promising for detecting H₂O₂ because of their advantages, such as easy miniaturization, rapid response, simple instrumentation, and high specificity and sensitivity. The natural concentration of H₂O₂ varies from micromolar (μM) to tens of millimolar (mM) [5]. While various techniques exist for H₂O₂ determination, such as chromatography [6], chemiluminescence [7], colorimetry [8], and titrimetric analysis [8], these methods are often complex, expensive, and time consuming. In recent years, many electrochemical approaches have been developed to determine low concentrations of H₂O₂ in a high-throughput fashion in fast, simple, reliable, and inexpensive ways [8–10].

Electrochemical sensors are suitable for various matrices, require minimal sample preparation, and exhibit high sensitivity and a wide concentration range with low limits of detection [11,12]. Enzymatic and non-enzymatic sensors have been developed for detecting H₂O₂ [13,14]. Enzymatic approaches exhibit excellent selectivity and sensitivity but lack stability, require complex and expensive immobilization processes, and are highly dependent

on experimental conditions. Therefore, developing non-enzymatic electrochemical H_2O_2 sensors is very interesting for various biomedical, industrial, and academic applications. Non-enzymatic electrochemical sensors have been developed by chemically modifying electrodes with nanomaterials, such as nanoparticles of noble metals, transition metals, metallic oxides/hydroxides, bimetallics/alloys, and carbon nanomaterials (CNT, graphene and its compounds) [5,15,16].

Among the promising metals for developing nanomaterials, titanium dioxide stands out. Titanium dioxide (TiO_2) is a transition metal oxide belonging to the category of n-type semiconductors, with its bandgap energy ranging from 2.9–3.2 eV [17], depending on the crystal phase [18]. Due to its high electrochemical activity, excellent mechanical and chemical stability, and exceptional capacity for organic molecule adsorption, TiO_2 is widely used in electrochemical sensors [19,20]. However, to further improve the sensing performance of TiO_2 , researchers are working on forming a hybrid structure with different materials with diverse functional properties. One such material extensively studied in electrochemical applications is multi-walled carbon nanotubes (MWCNTs), which possess remarkable physical and chemical properties, such as high electrical conductivity, large surface area, and high energy storage capacity [21]. Previous investigations have shown that modifying electrodes with MWCNTs substantially enhances the rates of electron and proton transfer, resulting in superior peak separation and enhanced electrode sensitivity compared to other types of modified electrodes [22,23]. Additionally, the anchoring of semiconductors' metal oxide particles onto MWCNTs with homogenous distribution has exhibited improved electronic properties, making it a promising platform for selective sensing and catalytic processes.

Among various nanocomposites, the TiO_2 /MWCNTs nanostructures [24] and other notable composites, such as TiO_2 /MWCNTs/Pt [25–27], $Au@TiO_2$ /MWCNT [28], $ZnS/Au_{10}/f$ -MWCNT [29], and PB- TiO_2 /CNT [30], have been reported to exhibit exceptional electrocatalytic activity toward hydrogen peroxide (H_2O_2) and other analytes in biosensing applications. However, it should be mentioned that the growth of complex nanostructures and deposition of catalytic nanoparticles, as previously demonstrated in the literature, typically requires sophisticated techniques such as electrochemical anodization, electrochemical deposition, or photo-induced deposition. Although these techniques have enabled the creation of intricate nanostructures, they can be both time consuming and resource intensive [31].

In this context, the sol–gel technique combined with hydrothermal synthesis has emerged as a promising approach for the preparation of nanometer-sized particles and materials with high specific surface area [32]. TiO_2 /MWCNT nanocomposites can be prepared using this technique, which shows potential for developing chemical and electrochemical sensors or promoting novel applications in biosensing [33] and photodetection [33] thanks to its unique three-dimensional network texture, high surface area, and exceptional electrocatalytic activity.

This study presents a novel sensor for detecting H_2O_2 that employs a TiO_2 /MWCNT/Nafion nanocomposite as a surface modifier for a glassy carbon electrode (GCE) in conjunction with cyclic voltammetry (CV). The sensor exhibits high sensitivity and a low detection potential for H_2O_2 . Notably, this is the first report on the use of TiO_2 /MWCNT/Nafion on GCE for electrochemical H_2O_2 detection in water using CV. Our findings indicate that the TiO_2 /MWCNT/Nafion nanocomposite holds promise for developing high-performance H_2O_2 sensors with a facile synthesis process, making it a viable candidate for creating sensors for various clinical and environmental applications.

2. Materials and Methods

2.1. Materials

All chemical reagents used in this study were not subjected to additional purification. Titanium (IV) isopropoxide ($TiIP$, 97.00%) and hydrochloric acid (HCl , 36.00%) were obtained from Sigma-Aldrich (St. Louis, MO, USA). Absolute ethanol (99.5%, CRQ Produ-

tos Químicos, Diadema, Brazil), isopropanol (Sciavico Comércio e Indústria Ltda, Belo Horizonte, Brazil), and sodium hydroxide micropellets (NaOH, Cromoline Química Fina, Diadema, Brazil). Multi-walled carbon nanotubes (MWCNTs) with an outer diameter of 8–25 nm and length ranging from 5.00 to 30.00 μm and a purity of $\geq 93\%$ were provided by the Nanomaterials Laboratory of the Department of Physics, UFMG. Nafion-117 was purchased from Sigma-Aldrich (Oakville, ON, USA).

2.2. Synthesis of TiO_2 Particles

The TiO_2 particles were prepared with modifications by the sol–gel method proposed by Ferreira-Neto, Elias et al. [20], represented in Figure 1. Initially, 750.00 μL of titanium isopropoxide (TiP) was slowly added to 100.00 mL of a mixture composed of ethanol–isopropanol [3:1 (*v/v*)] under magnetic stirring, which was maintained for three hours.

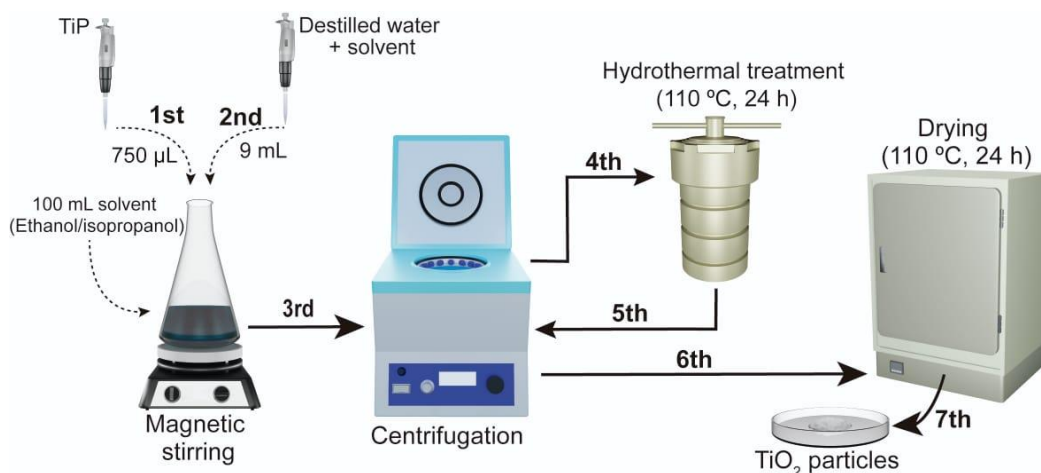


Figure 1. Diagram of preparation of TiO_2 nanoparticles by combined sol–gel and hydrothermal methods.

Subsequently, 9.00 mL of a mixture of deionized water and solvent (3.00 mL H_2O :6.00 mL of the ethanol–isopropanol solvent) were added dropwise to form TiO_2 particles through hydrolysis and condensation of titanium alkoxide species. After 2 h of magnetic stirring, the resulting colloidal suspension was centrifuged at 3500 rpm for 5 min and washed once with the solvent used in the reaction.

To crystallize the amorphous TiO_2 , the obtained material was resuspended in 32.00 mL of deionized water, then transferred to a 35.00 mL hermetic Teflon reactor and subjected to hydrothermal treatment at 110 $^\circ\text{C}$ for 24 h inside a flanged stainless steel hydrothermal reactor. After the hydrothermal treatment, the sample was centrifuged and washed twice with deionized water. Finally, the resulting precipitates were dried at 80 $^\circ\text{C}$ in an oven for 12 h.

2.3. Synthesis of $\text{TiO}_2/\text{MWCNT}$ Nanocomposite

The nanocomposite synthesis was adapted from the method Patel B.R. et al. proposed [34]. In this modified method, depicted in Figure 2, 100.00 mg of TiO_2 particles obtained in the previous step were combined with 50 mg of MWCNTs and added to 10.00 mL of 10 M NaOH solution in a microtube with a screw cap. The resulting mixture was sonicated for 30 min at 60 $^\circ\text{C}$ to ensure proper dispersion of the particles. Next, the mixture was transferred to an autoclave container made of stainless steel, lined with Teflon material, and subjected to hydrothermal treatment at 130 $^\circ\text{C}$ for 24 h.

After cooling to room temperature, the nanocomposite was washed with 1 L of ultrapure water to remove impurities and unreacted species. The sample was then neutralized to a pH of 7.00 using a 0.50 M HCl solution. To ensure the complete removal of impurities, the nanocomposites were subjected to centrifugation at 5000 rpm with adding 0.50 L of ultrapure water. This washing step was repeated three times.

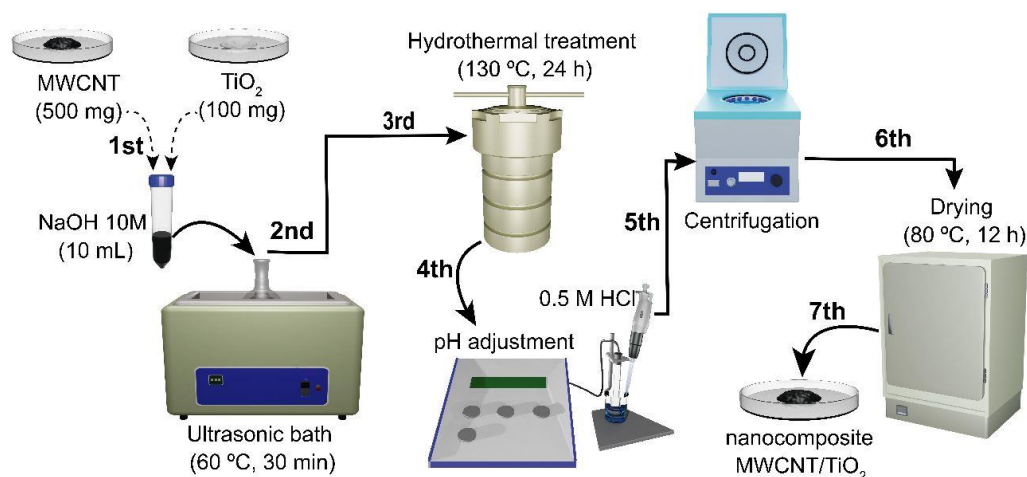


Figure 2. Schematic diagram of the preparation of TiO₂/MWCNT nanocomposite by hydrothermal method.

Finally, the nanocomposite was dried at 80 °C for 12 h to obtain a dry powder. The obtained material was named TiO₂/MWCNT and was used for further studies.

2.4. Materials Characterization

X-ray diffraction analysis (XRD) has been carried out on the Shimadzu diffractometer (model 6100; Kyoto, Japan) using a Co K α radiation source ($\lambda = 1.788 \text{ \AA}$, 40 kV/30 mA). Customary conditions included a 2θ scan from 10° to 70°, a 0.02° angular step, and a 1°/min scan speed. Data were converted to the Cu K α wavelength using PowDLL software v 2.7 [35]. The crystallographic phase identification was carried out by comparing the obtained patterns with JCPDS standards.

The samples' chemical structure and surface functional groups were analyzed using a Jasco FT/IR-4100 Fourier transform infrared spectrometer (FTIR) (Tokyo, Japan). The IR spectrum was recorded within the wavelength range of 4000 to 400 cm⁻¹.

The structure and surface morphology of the synthesized samples were analyzed using a scanning electron microscope (SEM), model JEOL JSM-6380LV (Tokyo, Japan), equipped with a Thermo Scientific Noran System SIX energy-dispersive X-ray spectrometer (EDS) (Waltham, MA, USA) operated at 20 kV.

Thermogravimetric measurements were conducted using a simultaneous thermal analyzer, the TGA-DSC Netzsch STA 449F3 Jupiter (Selb, Germany), in synthetic air from 30 °C to 900 °C at a heating rate of 10 °C/min.

2.5. Sensor Fabrication and Evaluation

A 3.00 mm diameter electrode was polished using 0.05 μm alumina slurry and thoroughly rinsed with distilled water to prepare the glassy carbon electrode for surface modification. A 10.00 μL dispersion of either MWCNTs or TiO₂/MWCNT nanocomposite in ultrapure water, each at a concentration of 1.00 mg/mL, was then added to the GCE surface. The active materials were immobilized with Nafion[®]-methanol (5.00% *w/v*) to create the MWCNT/Nafion/GCE and TiO₂/MWCNT/Nafion/GCE sensors. One of the unique features of Nafion is its ability to facilitate proton transfer from its sulfonic groups to the perfluorinated hydrophobic backbone, which results in the formation of a highly conductive medium for protons [10,36] to provide greater reticulation of the nanocomposites on the surface of the GCE.

Electrochemical sensing was conducted at room temperature using a three-electrode electrochemical cell (30.00 mL) consisting of the MWCNT/Nafion/GCE or TiO₂/MWCNT/Nafion/GCE as the working electrode, a Pt plate as the counter electrode, and Ag|AgCl as the reference electrode. The measurements were carried out using a portable bi-

potentiostat/galvanostat μ -Autolab Type III (Metrohm Autolab, Utrecht, The Netherlands) controlled by Nova 2.1 software.

The electrochemical sensing was performed in different H_2O_2 concentrations in a 0.10 M Britton–Robinson (B-R) buffer at pH 7.00 under constant magnetic stirring. After each triplicate, the solutions were homogenized by stirring for 30 s, and any electrogenerated products were removed from the electrode surface. For the addition–recovery experiments, standard solutions of H_2O_2 were prepared using 0.01 M ($\text{mol}\cdot\text{L}^{-1}$) stock solutions in ultrapure water ($R \geq 18.2 \text{ M}\Omega \text{ cm}$).

3. Results

3.1. Characterization of MWCNT and $\text{TiO}_2/\text{MWCNTs}$ Nanocomposite

Figure 3 shows the XRD diffraction patterns of both pristine MWCNT and $\text{TiO}_2/\text{MWCNT}$ nanocomposite. Although some peaks present low intensity, smoothing has been applied to distinguish them better.

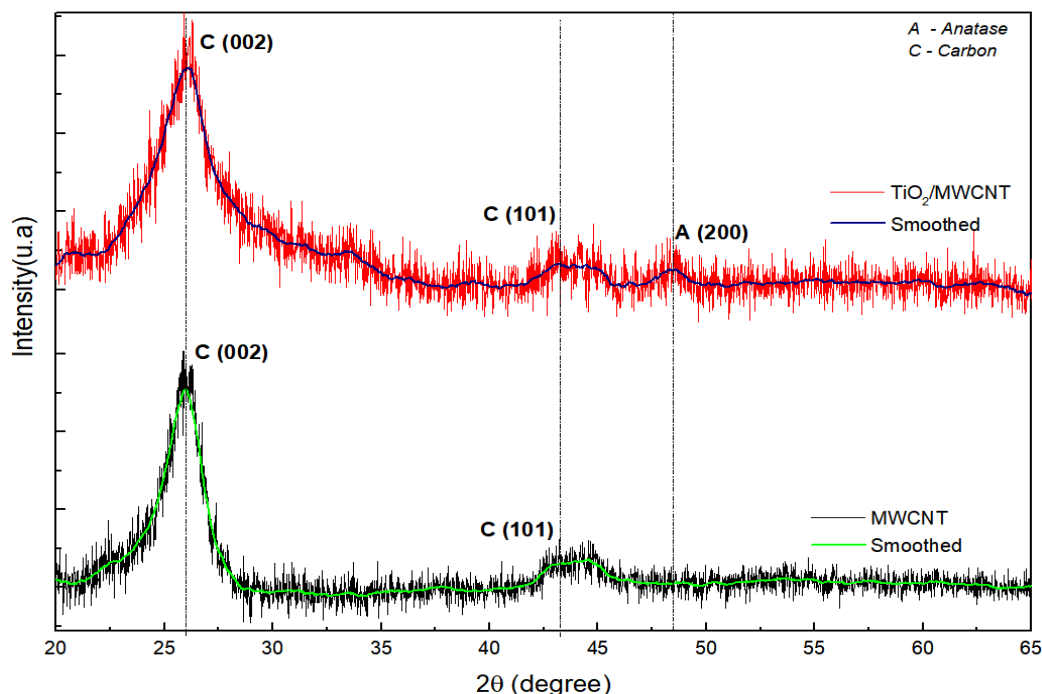


Figure 3. XRD patterns of pristine MWCNT and $\text{TiO}_2/\text{MWCNT}$ nanocomposite.

The XRD patterns of pristine MWCNTs show diffraction peaks of graphite structures at $2\theta = 25.8^\circ$ and 43.5° (JCPDS card 41-1487) corresponding to reflections from crystallographic planes (002), the spacing between adjacent graphite layers, and ordering within the plane (100), respectively.

In addition to the diffraction peaks related to pristine MWCNTs, the MWCNT/ TiO_2 nanocomposite exhibits a diffraction peak at $2\theta = 48.2^\circ$ related to the (200) plane, indicating the formation of the anatase phase of TiO_2 (JCPDS card no. 21-1272). The significant broadening of the peak indicates the nanometric characteristic of the TiO_2 particles. Thus, the hydrothermal treatment employed was effective, as it promoted the crystallization of amorphous titania into the anatase phase.

An approximate measure of the crystallite size of the TiO_2 phase in the sample was determined using the well-known Scherrer equation [37], which is based on the full width at half maximum (FWHM) \AA obtained by a Gaussian function, diffraction angle θ and the wavelength λ associated with Cu $K\alpha$ radiation. The average crystallite size of anatase (200) was found to be 5.50 nm based on the broadening of its diffraction peak, where the FWHM is 1.63 \AA .

The FTIR spectra of pristine MWCNTs, bare TiO₂ particles, and TiO₂/MWCNT nanocomposite are shown in Figure 4.

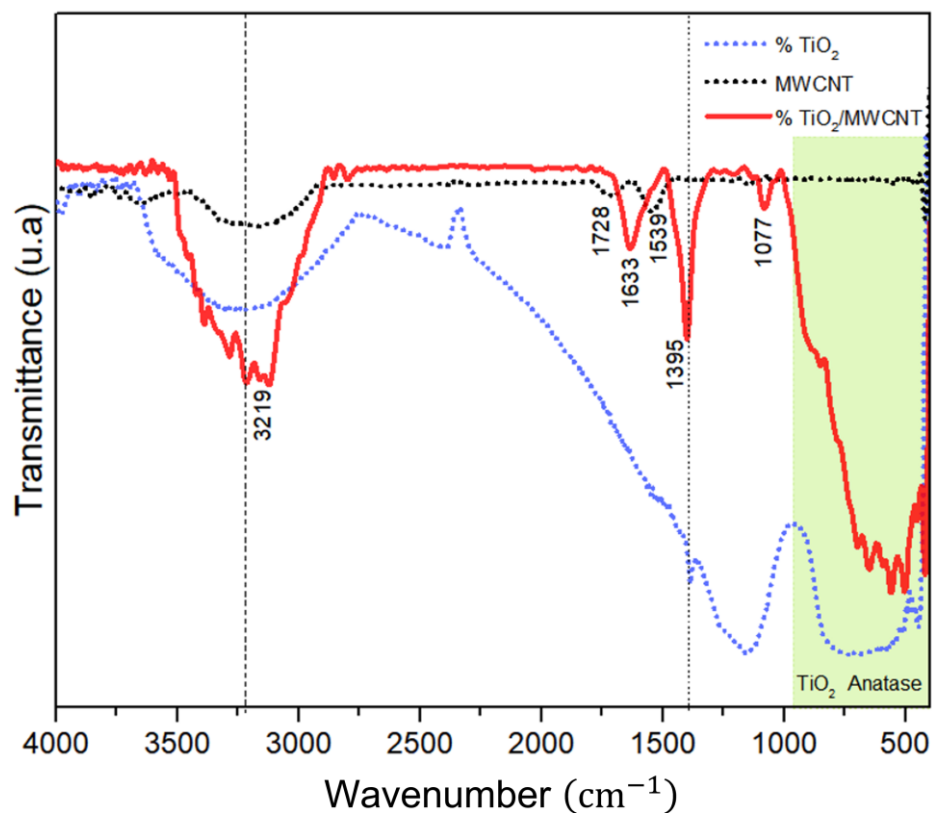


Figure 4. FTIR of MWCNT, TiO₂ particles, and TiO₂/MWCNTs nanocomposite.

The FTIR spectra of all samples showed a broad absorption band in the range of 3000 to 3500 cm⁻¹, centered at 3219 cm⁻¹, attributed to the O-H stretching vibration and the surface adsorbed water [38]. In the MWCNTs' FTIR spectrum, distinct peaks were observed at 1539, 1728, and 3219 cm⁻¹. The peak at 1539 cm⁻¹ confirmed the presence of graphitic carbon bonds (C=C stretching vibration), while the peak at 1728 cm⁻¹ indicated the presence of carbonyl (C=O) functional groups [39,40].

The FTIR spectrum of bare TiO₂ particles shows a broad band of 1000 to 400 cm⁻¹, which can be attributed to various stretching vibrations, including Ti-O and O-Ti-O bonds [41]. However, in the FTIR spectrum of the TiO₂/MWCNT nanocomposite, in addition to the Ti-O and O-Ti-O bonds, the presence of Ti-O-C and Ti-O-C=O bonds is observed, indicating an interaction between TiO₂ particles and the MWCNTs [42]. Furthermore, the anatase titania phase, as revealed by XRD analysis, contributes to the observed band [43,44]. Both the nanocomposite and bare TiO₂ particles exhibit a distinct band ~1395 cm⁻¹ corresponding to TiO₂ lattice vibrations [45,46]. In addition, the FTIR spectrum of the TiO₂/MWCNT nanocomposite also displays a peak at 1633 cm⁻¹, representing the deformative vibration of the Ti-OH stretching mode and the OH stretch of adsorbed water. Moreover, a band at 1100 cm⁻¹ has been attributed to alkoxy C-O stretching vibrations within the nanocomposite [47].

Thermogravimetric analysis was used to investigate the thermal stability of the studied materials. According to Figure 5, it can be observed that the MWCNT shows a mass loss caused by the oxidation of the nanotubes with a peak temperature at 575 °C, which agrees with values reported in the literature ranging from 550–650 °C [48]. The stability was achieved with a residue of 3.50%, resulting from the remaining catalysts from the synthesis of the nanotubes (MWCNT), as reported by the supplier of this material.

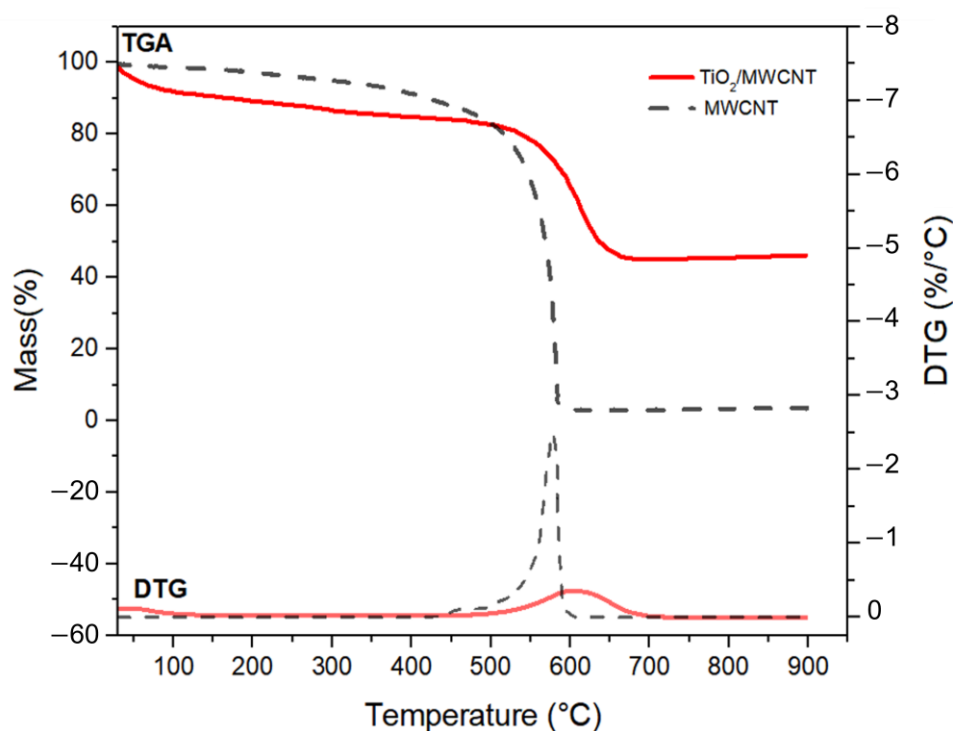


Figure 5. TG and DTG curves for pristine MWCNT and $\text{TiO}_2/\text{MWCNT}$ nanocomposite.

The $\text{MWCNT}/\text{TiO}_2$ nanocomposite exhibited a mass loss of 5.00% up to 100 °C, which can be attributed to adsorbed water on the material's surface—this mass loss results from the desorption of the water molecules from the nanocomposite. Between the temperature range of 100 and 450 °C, a further mass loss of approximately 8.00% was observed. This additional mass loss is believed to be caused by the decomposition of oxygenated groups that were incorporated into the MWCNTs during the synthesis process of the nanocomposite [49]. The presence of these oxygenated groups provides evidence for the bonding mechanism between TiO_2 and MWCNT, suggesting that the bonding occurs through the involvement of these functional groups. This bonding interaction between TiO_2 and MWCNT is further supported by the presence of Ti-O-C and Ti-O-C=O bonds, as observed in FTIR analysis.

Furthermore, it was observed that the temperature range at which significant mass loss occurs because of the oxidation of nanotubes is between 500–690 °C. This can be easily seen in the DTG curve. The constant levels observed in the TGA curve after 690 °C indicate that the nanotubes underwent complete oxidation. The residue reflects the percentage of TiO_2 present in the nanocomposite: approximately 41.50%.

The morphology of pristine MWCNT and $\text{MWCNT}/\text{TiO}_2$ nanocomposite samples were evaluated using SEM. Figure 6a shows that the pristine MWCNT has a smooth surface with entangled tube bundles. In Figure 6b–d, it can be observed that the $\text{MWCNT}/\text{TiO}_2$ has morphology like the undecorated MWCNTs, i.e., no particles that could be attributed to TiO_2 were marked.

The results from the EDS analysis, as shown in Figure 7, support the presence of titanium in the nanocomposite and its successful integration into the carbon nanotube matrix. These findings are consistent with the XRD and FTIR analysis results.

The EDX analysis of the $\text{TiO}_2/\text{MWCNT}$ nanocomposite demonstrated its atomic percent (at.%) and weight percent (w.%) composition. The analysis results are as follows: carbon (C)—73.50% (at.%) and 86.72% (w.%), titanium (Ti)—9.22% (at.%) and 8.17% (w.%), and oxygen (O)—17.28% (at.%) and 5.11% (w.%). These findings validate its chemical composition.

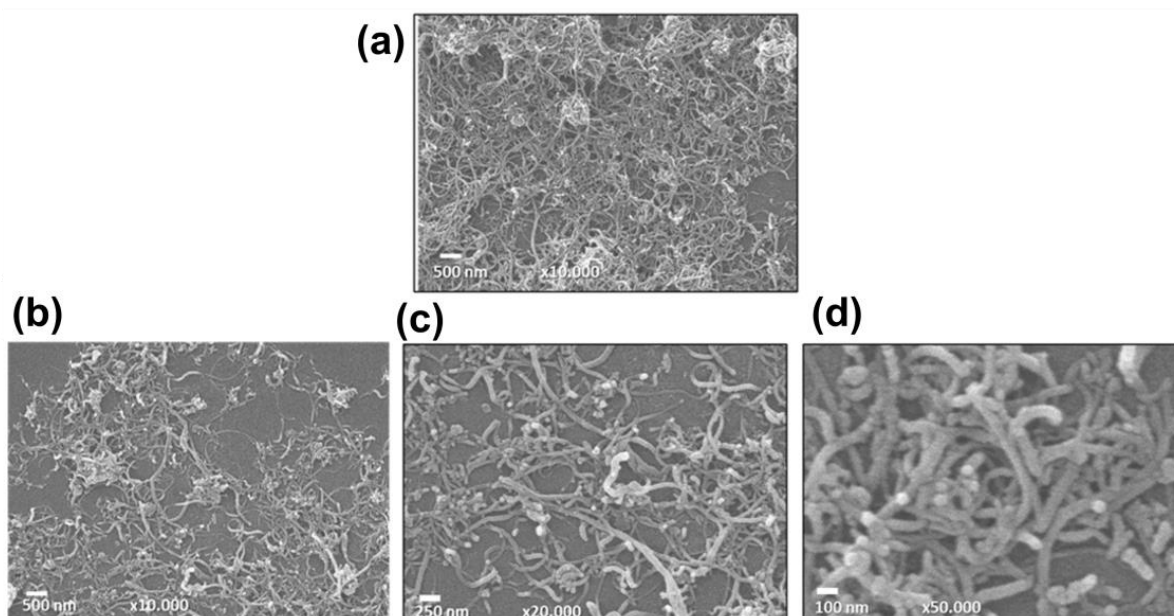


Figure 6. SEM images of pristine MWCNT (a) and TiO₂/MWCNT nanocomposite (b–d). Scale bars in (a,b) 500.00 nm, (c) 250.00 nm, and (d) 100.00 nm.

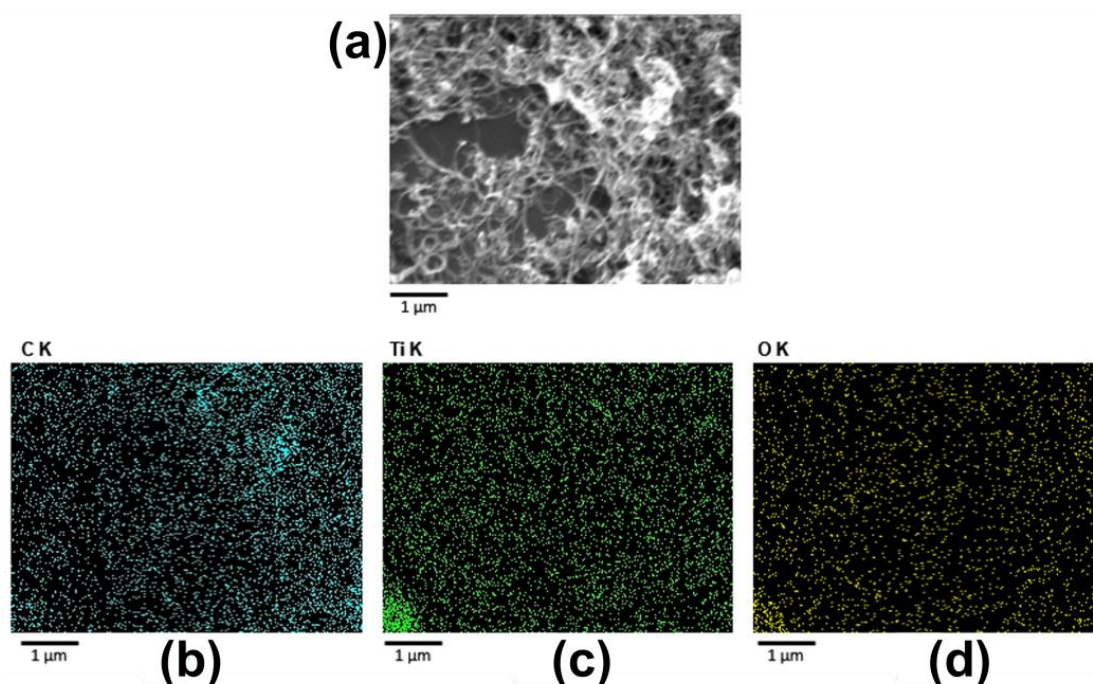


Figure 7. SEM image of the MWCNT/TiO₂ nanocomposite (a) and corresponding EDS elemental mapping with separate maps shown for (b) C, (c) Ti, and (d) O.

3.2. Electrochemical Behavior of GCE, MWCNT/Nafion, and TiO₂/MWCNT/Nafion-Modified GCEs

The electrocatalytic activity of modified working electrodes was examined by measuring the cyclic voltammograms (CVs) in 0.50 M H₂SO₄ within the potential range of −0.5 to 1.5 V vs. Ag|AgCl at a scan rate of 50 mVs^{−1}. As depicted in Figure 8a, the unmodified GCE was determined to be electrochemically inactive under these conditions, which aligns with the earlier observations reported by Benck et al. [50]. The CV of the bare CGE displayed no redox pair, resulting in a narrow and almost flat line in the graph.

This implies that no electrochemical reactions were taking place on the surface of the CGE electrode under the specified conditions.

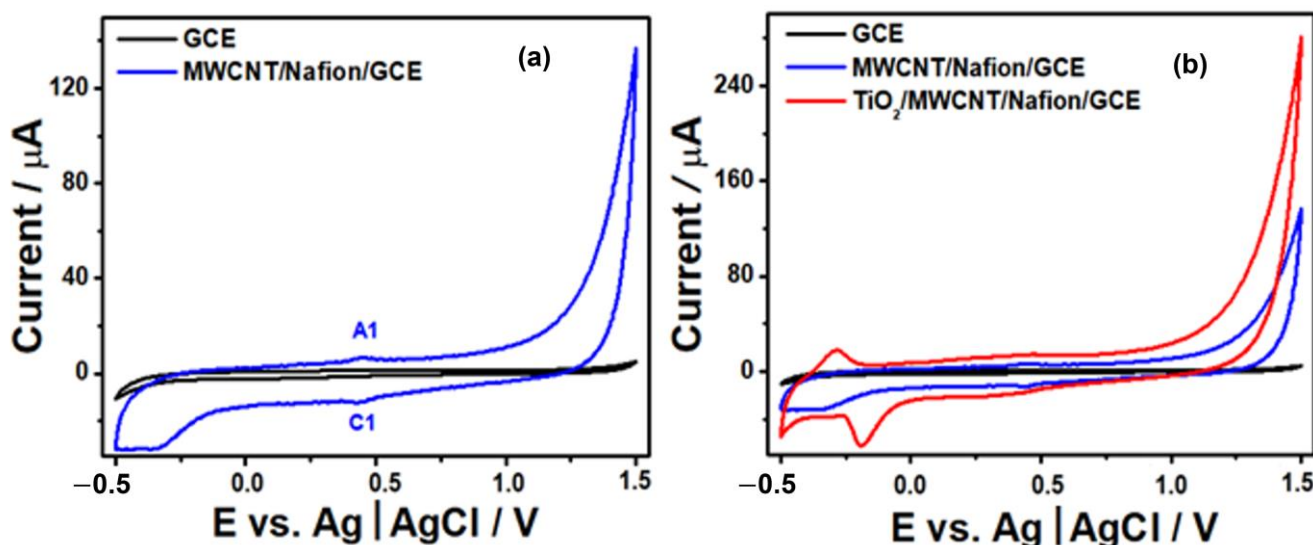


Figure 8. Cyclic voltammograms measured in 0.50 M H_2SO_4 within the potential range of -0.5 V to 1.5 V vs. Ag | AgCl at a scan rate of 50 mVs^{-1} using bare GCE, MWCNT/Nafion-modified GCE (a), and $\text{TiO}_2/\text{MWCNT}/\text{Nafion}$ -modified GCE (b).

0.5 V to 1.5 V vs. Ag | AgCl at a scan rate of 50 mVs^{-1} using bare GCE, MWCNT/Nafion-modified GCE (a), and $\text{TiO}_2/\text{MWCNT}/\text{Nafion}$ -modified GCE (b).

However, in Figure 8a, the modification of the CGE electrode with MWCNT altered the electrochemical profile of the surface, broadening the area of the voltammogram, as the carbon nanotubes provided a surface and electroactive increment. In addition, two peaks, A1 and C1, are observed, which correlate with the redox reactions of metallic iron resulting from the catalyst used to synthesize MWCNTs [51,52]. Notably, the potential scan toward more negative values for the GCE/MWCNT/ TiO_2 electrode gives rise to redox current peaks in the potential region between -0.5 and 0.0 V, which may be associated with the oxidation/reduction in Ti ions [53–56].

Moreover, the presence of oxygenated functional groups, such as hydroxyls (OH) and carbonyls (C=O), in the $\text{TiO}_2/\text{MWCNT}$ nanocomposite plays a significant role in its electrochemical behavior. These functional groups contribute to increased adsorption capacity for species and provide additional active sites for the adsorption of molecules and ions. Consequently, electrochemical reactions, including the oxidation of H_2O_2 , can take place more efficiently. This makes the modified GCE electrode an up-and-coming candidate for H_2O_2 -sensing applications where accurate and sensitive detection of H_2O_2 is required [57–59].

3.3. Evaluation of $\text{TiO}_2/\text{MWCNT}/\text{Nafion}/\text{GCE}$ Electrode as an Electrochemical Sensor for H_2O_2 Determination

The electrocatalytic activity of the $\text{TiO}_2/\text{MWCNT}/\text{Nafion}/\text{GCE}$ sensor toward the oxidation of H_2O_2 was investigated by CV. Figure 9a shows the cyclic voltammograms of the electrode in a Britton–Robinson (B-R) buffer solution at pH 7, under a potential scan range of -0.2 V to 1.0 V, in the absence of and after successive additions of hydrogen peroxide (from 0 up to $120 \mu\text{M}$) to the cell solution, and the corresponding calibration plot.

The cyclic voltammograms demonstrated the direct proportionality of the peak current to H_2O_2 concentration within 14.00 – $120.00 \mu\text{M}$. The linear regression equation illustrated $I_p (\mu\text{A}) = 1.0145x - 0.0346$, ($R^2 = 0.9985$) (Figure 9b). The detection limits (LD) and quantification limits (LQ) were calculated according to the recommendations of the IUPAC

as three times the standard deviation of the blank signal—Britton–Robinson buffer—(σ_B) divided by the slope of the calibration curve (m): $LD = 3 \sigma_B/m$. The LQs were calculated similarly, with 10 replacing 3 in each equation, i.e., $LQ = 10 \sigma_B/m$. Therefore, the LD and LQ limits obtained were $4.00 \mu\text{M}$ and $14.00 \mu\text{M}$, respectively.

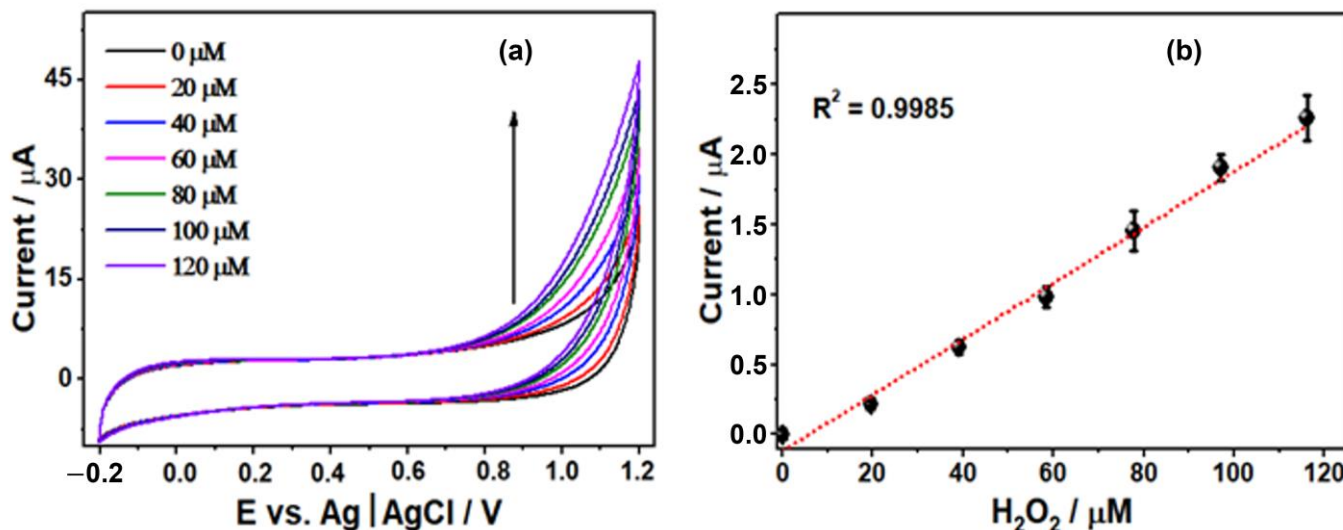


Figure 9. (a) Cyclic voltammograms of the $\text{TiO}_2/\text{MWCNT}/\text{Nafion}/\text{GCE}$ to successive addition of H_2O_2 concentrations (0.00 up to 120.00 μM) into a continuously stirred B-R buffer solution, $\text{pH} = 7.00$. (b) The calibration curve of current vs. H_2O_2 concentration.

The fabricated sensor's accuracy was evaluated using the standard addition method, in distilled deionized water, at three different concentration levels of H_2O_2 (20.00, 40.00, and 60.00 μM) Britton–Robinson buffer solution at a pH of 7.00, using cyclic voltammetry.

The results are presented in Table 1, demonstrating a range of variation between 67.30% and 101.90%. Our findings indicate that this analytical method is only sufficiently accurate for concentrations greater than 20.00 μM .

Table 1. Results for the recovery study in distilled-deionized water at three concentration levels for H_2O_2 in Britton–Robinson buffer solution at pH 7.00.

Added (μM)	Found (μM)	Recovery (%)
20.00	13.20 ± 0.11	67.30
40.00	36.02 ± 0.25	92.30
60.00	59.50 ± 0.12	101.90

A comparison between the $\text{TiO}_2/\text{MWCNT}/\text{Nafion}/\text{GCE}$ electrode and other GCE-modified electrodes reported in the literature is presented in Table 2. Our results align with those of other studies, indicating that this electrode coating is suitable for detecting H_2O_2 . Furthermore, it is worth noting that the $\text{TiO}_2/\text{MWCNT}/\text{Nafion}/\text{GCE}$ electrode can be produced with fewer laborious steps than in some of the previous works.

Considering that hydrogen peroxide concentrations typically range from micromolar for in vivo conditions and residual levels in foodstuffs and drinking water to tens of millimolar for bleaching applications and molar for waste treatment applications [67], the $\text{TiO}_2/\text{MWCNT}/\text{Nafion}/\text{GCE}$ has the potential to determine H_2O_2 levels in water.

Table 2. Comparison of the proposed sensor with the recently reported H₂O₂ sensors.

Modifier Material	Method	LD (μM)	References
MWCNT-POMAF	Amp	0.33	[60]
Co/MWCNT	DPV	1.84	[61]
AuNPs/PSi/Nafion	LSV	14.84	[62]
AuNPs/PSi/Nafion	SWV	15.16	[62]
Hb/MoS	CV	6.70	[63]
Ag/MWCNT	DPV	3.30	[61]
MoS ₂	CV	1.13	[64]
Au@TiO ₂ /MWCNT	DPV	1.40	[28]
PB-TiO ₂ /fCN	CA	0.088	[30]
TiO ₂ /MWCNT	Amp	0.40	[28]
Ni(OH) ₂ /ERGO-MWNT	Amp	4.00	[65]
Ag@TiO ₂	CV	0.83	[66]
MWCNT/TiO ₂	CV	4.00	This work

Abbreviations used: Amp (amperometry), DPV (differential pulse voltammetry), LSV (linear sweep voltammetry), SWV (square wave voltammetry), CV (cyclic voltammetry), CA (chronoamperometry), MWCNT-POMAF (multi-walled carbon nanotubes functionalized with polyoxometalate), Co/MWCNT (cobalt/multi-walled carbon nanotubes), AuNPs/PSi/Nafion (gold nanoparticles/porous silicon/Nafion), AuNPs/PSi/Nafion (gold nanoparticles/porous silicon/Nafion), Hb/MoS (hemoglobin/molybdenum sulfide), Ag/MWCNT (silver/multi-walled carbon nanotubes), MoS₂ (molybdenum disulfide), Au@TiO₂/MWCNT (gold@titanium dioxide/multi-walled carbon nanotubes), PB-TiO₂/fCN (phosphate buffer-titanium dioxide/functionalized carbon nitride), TiO₂/MWCNT (titanium dioxide/multi-walled carbon nanotubes), Ni(OH)₂/ERGO-MWNT (nickel hydroxide/electrochemically reduced graphene oxide–multi-walled carbon nanotubes), Ag@TiO₂ (silver@titanium dioxide), MWCNT/TiO₂ (multi-walled carbon nanotubes/titanium dioxide).

4. Conclusions

In summary, a novel H₂O₂ voltammetric sensor has been developed by modifying a glassy carbon electrode (GCE) with a TiO₂/MWCNT/Nafion nanocomposite synthesized using a facile hydrothermal route. Incorporating semiconducting TiO₂ nanoparticles and highly conducting MWCNTs synergistically enhanced the sensor's performance toward H₂O₂ detection, surpassing the performance of both bare GCE and MWCNT/Nafion-modified GCE electrodes. The proposed modified electrode successfully detected and determined H₂O₂ concentrations in water ranging from 14.00–120.00 μM, with a detection limit of 4.00 μM.

These findings represent a significant advancement in the design and fabrication of highly efficient H₂O₂-based sensor devices and have important implications for various applications such as water treatment, food safety, and biomedical diagnostics. Using the TiO₂/MWCNT/Nafion nanocomposite as a sensing material holds great promise for developing cost-effective, reliable, and sensitive H₂O₂ sensors with a wide range of detection capabilities.

Further research could explore the potential of this novel sensor platform for other analytes and environmental conditions, paving the way for the development of next-generation sensing technologies. However, it is essential to note that extensive testing and validation of the sensor's performance under different conditions will be necessary to ensure its practical applicability before commercialization.

Author Contributions: R.H.d.O. and D.A.G. conceived and designed the experiments and performed the experiments; R.H.d.O. analyzed the data and wrote the paper; D.D.d.R. and D.A.G. contributed with materials, supervision, and review. All authors have read and agreed to the published version of the manuscript.

Funding: This study was financed in part by the Coordenação de Aperfeiçoamento de Pessoal de Nível Superior—Brasil (CAPES)—Finance Code 001.

Institutional Review Board Statement: Not applicable.

Informed Consent Statement: Not applicable.

Data Availability Statement: Not applicable.

Acknowledgments: We are very grateful for the financial support from CAPES. We also would like to thank INCT Nanocarbono for supporting this work.

Conflicts of Interest: The authors declare no conflict of interest.

References

1. Mattos, I.L.D.; Shiraishi, K.A.; Braz, A.D.; Fernandes, J.R. Peróxido de Hidrogênio: Importância e Determinação. *J. Química Nova* **2003**, *26*, 373–380. [[CrossRef](#)]
2. Geiszt, M.; Leto, T.L. The Nox Family of Nad (P) H Oxidases: Host Defense and Beyond. *J. Biol. Chem.* **2004**, *279*, 51715–51718. [[CrossRef](#)] [[PubMed](#)]
3. Giorgio, Marco, Mirella Trinei, Enrica Migliaccio, and Pier Giuseppe Pelicci. Hydrogen Peroxide: A Metabolic by-Product or a Common Mediator of Ageing Signals? *J. Nat. Rev. Mol. Cell Biol.* **2007**, *8*, 722–728. [[CrossRef](#)] [[PubMed](#)]
4. Martinez-Calatayu, J. *Flow Injection Analysis of Pharmaceuticals: Automation in the Laboratory*; CRC Press: Boca Raton, FL, USA, 1996.
5. Dhara, K.; Mahapatra, D.R. Recent Advances in Electrochemical Nonenzymatic Hydrogen Peroxide Sensors Based on Nanomaterials: A Review. *J. Mater. Sci.* **2019**, *54*, 12319–12357. [[CrossRef](#)]
6. Mingrui, S.; Junli, W.; Baiyang, C.; Lei, W. A Facile, Nonreactive Hydrogen Peroxide (H₂O₂) Detection Method Enabled by Ion Chromatography with Uv Detector. *Anal. Chem.* **2017**, *89*, 11537–11544.
7. Al Lawati, H.A.; Hassanzadeh, J.; Bagheri, N. A Handheld 3d-Printed Microchip for Simple Integration of the H₂O₂-Producing Enzymatic Reactions with Subsequent Chemiluminescence Detection: Application for Sugars. *J. Food Chem.* **2022**, *383*, 132469. [[CrossRef](#)] [[PubMed](#)]
8. Lu, J.; Zhang, H.; Li, S.; Guo, S.; Shen, L.; Zhou, T.; Zhong, H.; Wu, L.; Meng, Q.; Zhang, Y. Oxygen-Vacancy-Enhanced Peroxidase-Like Activity of Reduced Co₃O₄ Nanocomposites for the Colorimetric Detection of H₂O₂ and Glucose. *J. Inorg. Chem.* **2020**, *59*, 3152–3159. [[CrossRef](#)]
9. Ahmad, T.; Iqbal, A.; Halim, S.A.; Uddin, J.; Khan, A.; El Deeb, S.; Al-Harrasi, A. Recent Advances in Electrochemical Sensing of Hydrogen Peroxide (H₂O₂) Released from Cancer Cells. *Nanomaterials* **2022**, *12*, 1475. [[CrossRef](#)]
10. Tran, H.V.; Huynh, C.D.; Tran, H.V.; Piro, B. Cyclic Voltammetry, Square Wave Voltammetry, Electrochemical Impedance Spectroscopy and Colorimetric Method for Hydrogen Peroxide Detection Based on Chitosan/Silver Nanocomposite. *Arab. J. Chem.* **2018**, *11*, 453–459. [[CrossRef](#)]
11. Natinan, B.; Baeumner, A.J. Combining Electrochemical Sensors with Miniaturized Sample Preparation for Rapid Detection in Clinical Samples. *Sensors* **2015**, *15*, 547–564.
12. Aicheng, C.; Chatterjee, S. Nanomaterials Based Electrochemical Sensors for Biomedical Applications. *J. Chem. Soc. Rev.* **2013**, *12*, 5425–5438.
13. Kamyabi, M.; Hajari, N. Low Potential and Non-Enzymatic Hydrogen Peroxide Sensor Based on Copper Oxide Nanoparticle on Activated Pencil Graphite Electrode. *J. Braz. Chem. Soc.* **2017**, *28*, 808–818. [[CrossRef](#)]
14. Nestor, U.; Frodouard, H.; Theoneste, M. A Brief Review of How to Construct an Enzyme-Based H₂O₂ Sensor Involved in Nanomaterials. *J. Adv. Nanoparticles* **2020**, *10*, 1–25.
15. Portorreal-Bottier, A.; Gutiérrez-Tarriño, S.; Calvente, J.J.; Andreu, R.; Roldán, E.; Oña-Burgos, P.; Olloqui-Sariego, J.L. Enzyme-Like Activity of Cobalt-Mof Nanosheets for Hydrogen Peroxide Electrochemical Sensing. *Sens. Actuators B Chem.* **2022**, *368*, 132129. [[CrossRef](#)]
16. Pang, P.; Yang, Z.; Xiao, S.; Xie, J.; Zhang, Y.; Gao, Y. Nonenzymatic Amperometric Determination of Hydrogen Peroxide by Graphene and Gold Nanorods Nanocomposite Modified Electrode. *J. Electroanal. Chem.* **2014**, *727*, 27–33. [[CrossRef](#)]
17. Bai, J.; Zhou, B. Titanium Dioxide Nanomaterials for Sensor Applications. *Chem. Rev.* **2014**, *114*, 10131–10176. [[CrossRef](#)] [[PubMed](#)]
18. Linsebigler, A.L.; Lu, G.; Yates, J.T., Jr. Photocatalysis on TiO₂ Surfaces: Principles, Mechanisms, and Selected Results. *J. Chem. Rev.* **1995**, *95*, 735–758. [[CrossRef](#)]
19. Hu, Y.; Tsai, H.L.; Huang, C.L. Phase Transformation of Precipitated TiO₂ Nanoparticles. *Mater. Sci. Eng. A* **2003**, *344*, 209–214. [[CrossRef](#)]
20. Ferreira-Neto, E.P.; Ullah, S.; Simões, M.B.; Perissinotto, A.P.; de Vicente, F.S.; Noeske, P.-L.M.; Ribeiro, S.J.L.; Rodrigues-Filho, U.P. Solvent-controlled deposition of titania on silica spheres for the preparation of SiO₂@TiO₂ core@shell nanoparticles with enhanced photocatalytic activity. *Colloids Surf. A Physicochem. Eng. Asp.* **2019**, *570*, 293–305. [[CrossRef](#)]
21. Andrews, R.; Jacques, D.; Qian, D.; Rantell, T. Multiwall Carbon Nanotubes: Synthesis and Application. *J. Acc. Chem. Res.* **2002**, *35*, 1008–1017. [[CrossRef](#)]
22. You, J.M.; Jeong, Y.N.; Ahmed, M.S.; Kim, S.K.; Choi, H.C.; Jeon, S. Reductive Determination of Hydrogen Peroxide with Mwcnts-Pd Nanoparticles on a Modified Glassy Carbon Electrode. *Biosens. Bioelectron.* **2011**, *26*, 2287–2291. [[CrossRef](#)] [[PubMed](#)]
23. Tavakkoli, H.; Akhond, M.; Ghorbankhani, G.A.; Absalan, G. Electrochemical Sensing of Hydrogen Peroxide Using a Glassy Carbon Electrode Modified with Multiwalled Carbon Nanotubes and Zein Nanoparticle Composites: Application to Hepg2 Cancer Cell Detection. *Microchim. Acta* **2020**, *187*, 105.

24. Qiu, J.; Zhang, S.; Zhao, H. Recent Applications of TiO₂ Nanomaterials in Chemical Sensing in Aqueous Media. *Sens. Actuators B Chem.* **2011**, *160*, 875–890. [[CrossRef](#)]
25. Pang, X.; He, D.; Luo, S.; Cai, Q. An Amperometric Glucose Biosensor Fabricated with Pt Nanoparticle-Decorated Carbon Nanotubes/TiO₂ Nanotube Arrays Composite. *Sens. Actuators B Chem.* **2009**, *137*, 134–138. [[CrossRef](#)]
26. Santangelo, S.; Messina, G.; Faggio, G.; Donato, A.; De Luca, L.; Donato, N.; Bonavita, A.; Neri, G. Micro-Raman Analysis of Titanium Oxide/Carbon Nanotubes-Based Nanocomposites for Hydrogen Sensing Applications. *J. Solid State Chem.* **2010**, *183*, 2451–2455. [[CrossRef](#)]
27. Santangelo, S.; Faggio, G.; Messina, G.; Fazio, E.; Neri, F.; Neri, G. On the Hydrogen Sensing Mechanism of Pt/TiO₂/Cnts Based Devices. *Sens. Actuators B Chem.* **2013**, *178*, 473–484. [[CrossRef](#)]
28. Jiang, L.C.; Zhang, W.D. Electrodeposition of TiO₂ Nanoparticles on Multiwalled Carbon Nanotube Arrays for Hydrogen Peroxide Sensing. *J. Electroanal.* **2009**, *21*, 988–993. [[CrossRef](#)]
29. Naik, S.S.; Lee, S.J.; Theerthagiri, J.; Yu, Y.; Choi, M.Y. Rapid and Highly Selective Electrochemical Sensor Based on ZnS/Au-Decorated F-Multi-Walled Carbon Nanotube Nanocomposites Produced Via Pulsed Laser Technique for Detection of Toxic Nitro Compounds. *J. Hazard. Mater.* **2021**, *418*, 126269. [[CrossRef](#)]
30. Guerrero, L.A.; Fernández, L.; González, G.; Montero-Jiménez, M.; Uribe, R.; Díaz Barrios, A.; Espinoza-Montero, P.J. Peroxide Electrochemical Sensor and Biosensor Based on Nanocomposite of TiO₂ Nanoparticle/Multi-Walled Carbon Nanotube Modified Glassy Carbon Electrode. *Nanomaterials* **2020**, *10*, 64. [[CrossRef](#)]
31. Frontera, P.; Malara, A.; Stelitano, S.; Leonardi, S.G.; Bonavita, A.; Fazio, E.; Antonucci, P.; Neri, G.; Neri, F.; Santangelo, S. Characterisation and H₂O₂ Sensing Properties of TiO₂-Cnts/Pt Electro-Catalysts. *Mater. Chem. Phys.* **2016**, *170*, 129–137. [[CrossRef](#)]
32. Seck, E.I.; Doña-Rodríguez, J.M.; Melián, E.P.; Fernández-Rodríguez, C.; González-Díaz, O.M.; Portillo-Carrizo, D.; Pérez-Peña, J. Comparative Study of Nanocrystalline Titanium Dioxide Obtained through Sol–Gel and Sol–Gel–Hydrothermal Synthesis. *J. Colloid Interface Sci.* **2013**, *400*, 31–40. [[CrossRef](#)] [[PubMed](#)]
33. Kaur, J.; Vergara, A.; Rossi, M.; Gravagnuolo, A.M.; Valadan, M.; Corrado, F.; Conte, M.; Gesuele, F.; Giardina, P.; Altucci, C. Electrostatically Driven Scalable Synthesis of MoS₂–Graphene Hybrid Films Assisted by Hydrophobins. *RSC Adv.* **2017**, *7*, 50166–50175. [[CrossRef](#)]
34. Patel, B.R.; Imran, S.; Ye, W.; Weng, H.; Noroozifar, M.; Kerman, K. Simultaneous Voltammetric Detection of Six Biomolecules Using a Nanocomposite of Titanium Dioxide Nanorods with Multi-Walled Carbon Nanotubes. *Electrochim. Acta* **2020**, *362*, 137094. [[CrossRef](#)]
35. Kourkoumelis, N. PowDLL, a Reusable.Net Component for Interconverting Powder Diffraction Data: Recent Developments. *Powder Diffr. J.* **2013**, *28*, 137–148.
36. Li, S.; Noroozifar, M.; Kerman, K. Nanocomposite of Ferricyanide-Doped Chitosan with Multi-Walled Carbon Nanotubes for Simultaneous Senary Detection of Redox-Active Biomolecules. *J. Electroanal. Chem.* **2019**, *849*, 113376. [[CrossRef](#)]
37. Klung, H.P.; Alexander, L.E. *X-Ray Diffraction Procedures*; John Wiley Sons: New York, NY, USA, 1962; Volume 1, p. 974.
38. Zhang, Y.; Zhang, W.; Yang, K.; Yang, Y.; Jia, J.; Liang, Y.; Guo, L. Carbon Nano-Onions (Cnos)/TiO₂ Composite Preparation and Its Photocatalytic Performance under Visible Light Irradiation. *J. Environ. Eng.* **2020**, *146*, 04020009. [[CrossRef](#)]
39. Delekar, S.D.; Dhodamani, A.G.; More, K.V.; Dongale, T.D.; Kamat, R.K.; Acquah, S.F.; Dalal, N.S.; Panda, D.K. Structural and Optical Properties of Nanocrystalline TiO₂ with Multiwalled Carbon Nanotubes and Its Photovoltaic Studies Using Ru(li) Sensitizers. *ACS Omega* **2018**, *3*, 2743–2756. [[CrossRef](#)]
40. Bahgat, M.; Farghali, A.A.; El Roubay, W.M.A.; Khedr, M.H. Synthesis and Modification of Multi-Walled Carbon Nano-Tubes (Mwcnts) for Water Treatment Applications. *J. Anal. Appl. Pyrolysis* **2011**, *92*, 307–313. [[CrossRef](#)]
41. Ashoka, N.B.; Swamy, B.K.; Jayadevappa, H. Nanorod TiO₂ Sensor for Dopamine: A Voltammetric Study. *New J. Chem.* **2017**, *41*, 11817–11827. [[CrossRef](#)]
42. Wang, L.; Guo, J.; Dang, J.; Huang, X.; Chen, S.; Guan, W. Comparison of the Photocatalytic Performance of TiO₂/Ac and TiO₂/Cnt Nanocomposites for Methyl Orange Photodegradation. *Water Sci. Technol.* **2018**, *78*, 1082–1093. [[CrossRef](#)]
43. Lu, X.; Lv, X.; Sun, Z.; Zheng, Y. Nanocomposites of Poly(L-Lactide) and Surface-Grafted TiO₂ Nanoparticles: Synthesis and Characterization. *Eur. Polym. J.* **2008**, *44*, 2476–2481. [[CrossRef](#)]
44. Hashimoto, M.; Takadama, H.; Mizuno, M.; Kokubo, T. Enhancement of Mechanical Strength of TiO₂/High-Density Polyethylene Composites for Bone Repair with Silane-Coupling Treatment. *J. Mater. Res. Bull.* **2006**, *3*, 515–524. [[CrossRef](#)]
45. Muduli, S.; Lee, W.; Dhas, V.; Mujawar, S.; Dubey, M.; Vijayamohan, K.; Han, S.-H.; Ogale, S. Enhanced Conversion Efficiency in Dye-Sensitized Solar Cells Based on Hydrothermally Synthesized TiO₂–Mwcnt Nanocomposites. *ACS Appl. Mater. Interfaces* **2009**, *1*, 2030–2035. [[CrossRef](#)] [[PubMed](#)]
46. Mali, S.S.; Betty, C.A.; Bhosale, P.N.; Patil, P.S. Synthesis, Characterization of Hydrothermally Grown Mwcnt–TiO₂ Photoelectrodes and Their Visible Light Absorption Properties. *ECS J. Solid State Sci. Technol.* **2012**, *1*, M15. [[CrossRef](#)]
47. Stobinski, L.; Lesiak, B.; Kövér, L.; Tóth, J.; Biniak, S.; Trykowski, G.; Judek, J. Multiwall Carbon Nanotubes Purification and Oxidation by Nitric Acid Studied by the Ftir and Electron Spectroscopy Methods. *J. Alloys Compd.* **2010**, *501*, 77–84. [[CrossRef](#)]
48. Serp, P.; Corrias, M.; Kalck, P. Carbon Nanotubes and Nanofibers in Catalysis. *J. Appl. Catal. A Gen.* **2003**, *253*, 337–358. [[CrossRef](#)]
49. Datsyuk, V.; Kalyva, M.; Papagelis, K.; Parthenios, J.; Tasis, D.; Siokou, A.; Kallitsis, I.; Galiotis, C. Chemical Oxidation of Multiwalled Carbon Nanotubes. *Carbon* **2008**, *46*, 833–840. [[CrossRef](#)]

50. Benck, J.D.; Pinaud, B.A.; Gorlin, Y.; Jaramillo, T.F. Substrate Selection for Fundamental Studies of Electrocatalysts and Photoelectrodes: Inert Potential Windows in Acidic, Neutral, and Basic Electrolyte. *PLoS ONE* **2014**, *9*, e107942. [[CrossRef](#)]
51. Fayemi, O.E.; Adekunle, A.S.; Ebenso, E.E. Biosensors & Bioelectronics Metal Oxide Nanoparticles/Multi-Walled Carbon Nanotube Nanocomposite Modified Electrode for the Detection of Dopamine: Comparative Electrochemical Study. *J. Biosens. Bioelectron.* **2015**, *6*, 10–4172.
52. Poornajar, M.; Nguyen, N.T.; Ahn, H.J.; Büchler, M.; Liu, N.; Kment, S.; Zboril, R.; Yoo, J.E.; Schmuiki, P. Fe₂O₃ Blocking Layer Produced by Cyclic Voltammetry Leads to Improved Photoelectrochemical Performance of Hematite Nanorods. *J. Surf.* **2019**, *2*, 131–144. [[CrossRef](#)]
53. Marken, F.; Bhambra, A.S.; Kim, D.H.; Mortimer, R.J.; Stott, S.J. Electrochemical Reactivity of TiO₂ Nanoparticles Adsorbed onto Boron-Doped Diamond Surfaces. *Electrochem. Commun.* **2004**, *6*, 1153–1158. [[CrossRef](#)]
54. Yu, H.; Ma, J.; Zhang, Y.; Zhang, X.; Shi, W. Cyclic Voltammetry Studies of TiO₂ Nanotube Arrays Electrode: Conductivity and Reactivity in the Presence of H⁺ and Aqueous Redox Systems. *J. Electrochim. Acta* **2011**, *56*, 6498–6502. [[CrossRef](#)]
55. Hassaninejad-Darzi, S.K.; Shajie, F. A Sensitive Voltammetric Determination of Anti-Parkinson Drug Pramipexole Using Titanium Dioxide Nanoparticles Modified Carbon Paste Electrode. *J. Braz. Chem. Soc.* **2017**, *28*, 529–539. [[CrossRef](#)]
56. Silva-Galindo, G.; Zapata-Torres, M. Synthesis and Characterization of TiO₂ Thick Films for Glucose Sensing. *J. Biosens.* **2022**, *12*, 973. [[CrossRef](#)]
57. Palisoc, S.T.; Natividad, M.T.; De Jesus, N.; Carlos, J. Highly Sensitive Agnp/Mwcnt/Nafion Modified Gce-Based Sensor for the Determination of Heavy Metals in Organic and Non-Organic Vegetables. *Sci. Rep.* **2018**, *8*, 17445. [[CrossRef](#)] [[PubMed](#)]
58. Da Silva, E.P.; Araujo, M.D.; Kunita, M.H.; Matos, R.; Medeiros, R.A. Electrochemical Sensor Based on Multi-Walled Carbon Nanotubes and N-Doped TiO₂ Nanoparticles for Voltametric Simultaneous Determination of Benserazide and Levodopa. *J. Mol.* **2022**, *27*, 8614. [[CrossRef](#)]
59. Tarahomi, S.; Rounaghi, G.H.; Zavar, M.H.A.; Daneshvar, L. Electrochemical Sensor Based on TiO₂ Nanoparticles/Nafion Biocompatible Film Modified Glassy Carbon Electrode for Carbamazepine Determination in Pharmaceutical and Urine Samples. *J. Electrochem. Soc.* **2018**, *165*, B946. [[CrossRef](#)]
60. Mujica, M.L.; Sotomayor-Santander, I.; Hermosilla-Ibáñez, P.; Oyarzun-Ampuero, F.; Rodríguez, M.C.; Rivas, G.A.; Venegas-Yazigi, D.; Bollo, S. Mwcnt-Organoimido Polyoxomolybdate Hybrid Material: Analytical Applications for Amperometric Sensing of Hydrogen Peroxide. *Electroanalysis* **2021**, *33*, 2105–2114. [[CrossRef](#)]
61. Ohannesian, L.; Streeter, A. *Handbook of Pharmaceutical Analysis*; CRC Press: Boca Raton, FL, USA, 2001.
62. Rashed, M.A.; Harraz, F.A.; Faisal, M.; El-Toni, A.M.; Alsaïari, M.; Al-Assiri, M.S. Gold Nanoparticles Plated Porous Silicon Nanopowder for Nonenzymatic Voltammetric Detection of Hydrogen Peroxide. *Anal. Biochem.* **2021**, *615*, 114065. [[CrossRef](#)]
63. Liu, H.; Su, X.; Duan, C.; Dong, X.; Zhu, Z. A Novel Hydrogen Peroxide Biosensor Based on Immobilized Hemoglobin in 3d Flower-Like Mos₂ Microspheres Structure. *Mater. Lett.* **2014**, *122*, 182–185. [[CrossRef](#)]
64. Haritha, V.; Vijayan, A.; Kumar, S.S.; Rakhi, R. Voltammetric Determination of Hydrogen Peroxide Using Mos₂ Modified Glassy Carbon Electrodes. *Mater. Lett.* **2021**, *301*, 130258. [[CrossRef](#)]
65. Gao, W.; Tjiu, W.W.; Wei, J.; Liu, T. Highly Sensitive Nonenzymatic Glucose and H₂O₂ Sensor Based on Ni(OH)₂/Electroreduced Graphene Oxide–Multiwalled Carbon Nanotube Film Modified Glass Carbon Electrode. *Talanta* **2014**, *120*, 484–490. [[CrossRef](#)] [[PubMed](#)]
66. Khan, M.M.; Ansari, S.A.; Lee, J.; Cho, M.H. Novel Ag@TiO₂ Nanocomposite Synthesized by Electrochemically Active Biofilm for Nonenzymatic Hydrogen Peroxide Sensor. *Mater. Sci. Eng. C* **2013**, *33*, 4692–4999. [[CrossRef](#)] [[PubMed](#)]
67. Evans, S.A.; Elliott, J.M.; Andrews, L.M.; Bartlett, P.N.; Doyle, P.J.; Denuault, G. Doyle, and Guy Denuault. Detection of Hydrogen Peroxide at Mesoporous Platinum Microelectrodes. *Anal. Chem.* **2002**, *74*, 1322–1326. [[CrossRef](#)] [[PubMed](#)]

Disclaimer/Publisher’s Note: The statements, opinions and data contained in all publications are solely those of the individual author(s) and contributor(s) and not of MDPI and/or the editor(s). MDPI and/or the editor(s) disclaim responsibility for any injury to people or property resulting from any ideas, methods, instructions or products referred to in the content.